HHS Public Access

Author manuscript

Inhal Toxicol. Author manuscript; available in PMC 2016 August 15.

Published in final edited form as:

Inhal Toxicol. 2015 ; 27(5): 247–253. doi:10.3109/08958378.2015.1033570.

Generation and characterization of large-particle aerosols using a center flow tangential aerosol generator with a nonhuman-primate, head-only aerosol chamber

J. Kyle Bohannon[1], **Matthew G. Lackemeyer**[1], **Jens H. Kuhn**[1], **Jiro Wada**[1], **Laura Bollinger**[1], **Peter B. Jahrling**[1,2], and **Reed F. Johnson**[2,*]

[1]Integrated Research Facility at Fort Detrick, National Institute of Allergy and Infectious Diseases, National Institutes of Health, Fort Detrick, Frederick, Maryland, USA

[2]Emerging Viral Pathogens Section, National Institute of Allergy and Infectious Diseases, National Institutes of Health, Fort Detrick, Frederick, Maryland, USA

Abstract

Aerosol droplets or particles produced from infected respiratory secretions have the potential to infect another host through inhalation. These respiratory particles can be polydisperse and range from 0.05–500 μm in diameter. Animal models of infection are generally established to facilitate the potential licensure of candidate prophylactics and/or therapeutics. Consequently, aerosol-based animal infection models are needed to properly study and counter airborne infections. Ideally, experimental aerosol exposure should reliably result in animal disease that faithfully reproduces the modelled human disease. Few studies have been performed to explore the relationship between exposure particle size and induced disease course for infectious aerosol particles. The center flow tangential aerosol generator (CenTAG™) produces large-particle aerosols capable of safely delivering a variety of infectious aerosols to nonhuman primates within a Class III Biological Safety Cabinet (BSC) for establishment or refinement of nonhuman primate infectious disease models. Here we report the adaptation of this technology to the Animal Biosafety Level 4 (ABSL-4) environment for the future study of high-consequence viral pathogens and the characterization of CenTAG™-created sham (no animal, no virus) aerosols using a variety of viral growth media and media supplements.

[*]Address for correspondence: Reed F. Johnson, PhD: Emerging Viral Pathogens Section (EVPS), Division of Intramural Research (DIR), National Institute of Allergy and Infectious Diseases (NIAID), National Institutes of Health (NIH), B-8200 Research Plaza, Fort Detrick, Frederick, MD 21702, USA; Tel: +1-301-631-7255; Fax: +1-301-619-5029; johnsonreed@mail.nih.gov.

Declaration of Interest

The work was funded in part through Battelle Memorial Institute's prime contract with NIAID, under Contract No. HHSN272200700016I. J.K.B., J.W. and L.B. performed this work as employees of Battelle Memorial Institute. Subcontractors to Battelle Memorial Institute who performed this work are: J.H.K., an employee of Tunnell Government Services, Inc. and M.G.L., an employee of Lovelace Respiratory Research Institute, Inc. This work was supported in part by NIAID Division of Intramural Research.

Keywords

ABSL-4; Aerobiology; Aerosol; BSL-4; CenTAG; Large Particle

Introduction

Aerosol droplets of saliva and other respiratory secretions ranging from 0.05–500 μm in diameter can be generated from coughing, sneezing, talking, and exhalation. These droplets, or particles, are polydisperse and can carry microorganisms and/or virions (Gralton et al., 2011, Fennelly et al., 2004). Aerosol infection may occur by inhalation of such particles containing pathogens. Naturally occurring aerosol particles containing pathogens are studied for prophylactic and therapeutic development. Additionally, aerosol particles containing pathogens can be created deliberately, for instance by rogue or bioterrorist organizations in attempts to destabilize governments and their associated economies (Leffel and Reed, 2004, Egan et al., 2011, Huang et al., 2007). When clinical trials of therapeutic agents against infections from hazardous pathogens are not ethical or feasible, well-characterized inhalational animal disease models are frequently required to develop medical countermeasures in lieu of human efficacy data (Food and Drug Administration, 2014b, Food and Drug Administration, 2014a). Similar to conventional exposure (e.g., parenteral) to an infectious agent in an animal model of human disease, experimental aerosol exposure should reliably result in animal disease that faithfully reproduces the human condition (Aebersold, 2012, Food and Drug Administration, 2014b). Nonhuman primate (NHP) models are commonly the animal model of choice for studying the infectivity of inhaled infectious agents because 1) NHPs are more closely genetically related to humans than to laboratory animals of other species and 2) aerosol particles deposit within their respiratory tract in a comparable manner (Cheng et al., 2008, Raabe et al., 1988).

Few investigators have examined the cause-and-effect relationship of bioaerosol particle size and infectivity in NHPs while studying deposition patterns of specific size ranges, from 1 to 20 μm. To our knowledge, very minimal work, if any, has been done investigating that relationship using viral aerosol particles and comparing deposition patterns. Several studies of aerosolized particles containing *Bacillus anthracis* spores or *Francisella tularensis* demonstrated that the infectivity and associated lethality of inhaled aerosol particles is a function of particle size: the 50% lethal dose (LD_{50}) increased with particle size (1–24 μm in diameter) (Druett et al., 1953, Day and Berendt, 1972). While some pathogenic small particle aerosols may cause more lethal disease in many studies, the disease course may not accurately reflect what is documented in humans. However, some pathogenic large-particle aerosols may be more infectious due targeting of the nervous system, as observed with Venezuelan equine encephalitis virus (Thomas, 2013).

Most investigators studying NHP aerosol exposure models use small, monodisperse pathogen-containing particles ranging from 1–3 μm in diameter (May, 1973, Reed et al., 2011, Barnewall et al., 2012, Reed et al., 2005, Alves et al., 2010, Hartman et al., 2014, Nalca et al., 2010, Lee et al., 2013, Zumbrun et al., 2012, Yeager et al., 2012) to study disease progression. In general, small aerosol particles (<3 μm in diameter) penetrate to the

alveoli of the lungs and may promote more severe disease than large particles (7–10 μm in diameter) that deposit within the nasopharyngeal region, (e.g., nose, mouth, pharynx, and larynx). Therefore, animal models that employ small-particle aerosol exposure may not accurately recapitulate human upper respiratory-tract disease. Large-particle aerosol inoculation may provide an alternative method to develop improved animal models of human disease. In addition, mucociliary clearance can be studied with large-particle aerosols to determine and the impact on disease transmission by respiratory secretions. For reference, particles intermediate in size (3–6 μm in diameter) deposit within the tracheobronchial region (Cheng et al., 2008).

Through an understanding of regional deposition patterns and subsequent disease course within the NHP respiratory tract, the researcher controls the primary site of infection and picks the appropriate pathogen-exposure dose to study aerosol infectivity and morbidity/lethality (Hinds, 1999).

In experimental settings, aerosols are typically produced mechanically, using atomizers and nebulizers to generate the aerosol particles containing the pathogen. While the Collison nebulizer is a well-established small-particle aerosol generator (May, 1973), spinning-top aerosol generators are widely used to create larger particle aerosols (6–15 μm in diameter) (Roy et al., 2003, May, 1973, Davies and Cheah, 1984). Generally, these latter aerosol generators have a spinning top that is supported and driven by a compressed air source. The compressed air suspends the top and keeps it spinning indefinitely at a constant speed set by the researcher. A liquid feed needle mounted above the spinning top delivers inoculum or media onto the center of the top at a controlled rate. Once the liquid contacts the spinning top, the liquid spreads out to the periphery of the top and forms ligaments. These ligaments stretch until the surface tension is too great, resulting in the production of aerosol particles (BGI., 2005).

Unfortunately, the instability and difficultly with balancing the top at a specific height or speed raises significant safety concerns. Especially problematic is the possibility that the spinning top generator is jolted or manipulated while aerosolizing an infectious agent. The top could disengage, causing physical damage to the generator, the surroundings, or the researcher while possibly spreading pathogens. Additionally, the uneven spinning of the top would disrupt the principles of operation and cause the produced aerosol particles to become polydisperse. Spinning top generators are also not trivial to use inside of Class III Biosafety Cabinet (Class III BSC) in which dexterity is limited and biosafety is paramount. However, aerosol research is mandated to occur in a biosafety cabinet, preferably a Class III BSC, during the study of high-consequence Risk Group 3–4 Pathogens and/or Select Agents (Centers for Disease Control and Prevention and National Institutes of Health, 2009). To overcome these shortcomings and improve ease of use, shock-proof mounting was introduced, and generators were modified or adapted to fit into a biosafety cabinets (Young et al., 1974, Melton et al., 1991, Mitchell and Stone, 1982, Gussman, 1981, Ellison, 1967, May, 1966).

The Centered flow Tangential Aerosol Generator (CenTAG™) is a type of spinning top large-particle aerosol generator specifically designed for biocontainment research using

Class III BSCs (CH Technologies USA, 2013). It is based on a principle described in 1949 (Walton and Prewett, 1949) (Figure. 1). The spinning top is not suspended in air at variable levels as in other spinning top generators, but, rather, it is locked into place by a motor shaft. This fixed rotor positions the liquid inlet precisely and predictably above the spinning top. Shock-proof mountings or additional modifications are not necessary to stabilize the aerosol generator. The spinning top rotor speed is controlled electronically via a control panel. A syringe pump, which controls the liquid feed rate of the generator, delivers the liquid onto the center of the rapidly rotating spinning top through a small nozzle, which produces an aerosol by tangential shear force. Increasing liquid flow beyond optimal rates determined by the manufacturer will lead to the formation of a roughly annular sheet of liquid, which will break up into aerosol droplets ranging in size. The researcher monitors the spinning top through evenly spaced polycarbonate observation ports around the CenTAG™ plenum to correct liquid feed rates.

At optimal flow rates, transient liquid ligaments radiate from the edge of the top. Once a liquid ligament has grown to a critical length, nearly monodisperse main aerosol droplets separate from it. Surface tension causes the remainder of the liquid ligament to detach and break into polydisperse satellite aerosol droplets, which are much smaller than the primary aerosol droplets. The aerosol particles produced range from 5–12 μm in diameter and are somewhat polydisperse, having a particle distribution of smaller satellite aerosol particles simultaneously produced (Figure 2). The larger aerosol particles are separated from the satellite smaller aerosol particles by means of a siphon vacuum constructed around the central top, thus pulling the smaller aerosol particles away from the inlet aerosol chamber. Compared to earlier aerosol generators, the CenTAG™ provides improved operation and maintenance, ease of use within biocontainment, and controls aerosol concentrations in real time. In addition, viability of an infectious agent may improve during this aerosol generation process due to the diluent used, which increases particle size and reduces desiccation.

Here we describe how to successfully generate and deliver large-particle aerosols using CenTAG™ technology. Implementation of this new generator can be used for defining and further developing animal models to better recapitulate human disease for known and emerging pathogens.

Materials and Methods

Experiments were designed to generate large-aerosol particles from Dulbecco’s Modified Eagle Medium (DMEM) (Lonza, Walkersville, MD), Eagle’s Minimum Essential Medium (EMEM) (Lonza), Roswell Park Memorial Institute medium (RPMI) (Lonza,), and phosphate-buffered saline (PBS), (Life Technologies, Grand Island, NY). These liquids were selected as test suspensions because they are commonly used in the laboratory for virion stock production in standard tissue culture (media) or for final virion stock resuspension (PBS) (Earley and Johnson, 1988). Fetal bovine serum (FBS) was added to the liquid media at various concentrations because it is often used to supplement virus growth media and virions produced by certain viruses require protein for stability maintenance during aerosolization (Barnewall et al., 2012, Reed et al., 2005). Glycerol (Sigma-Aldrich, St. Louis, MO) was added to the media to change viscosity and to facilitate generation of larger

aerosol particles (Roy et al., 2003). For particle-size and particle-distribution testing purposes, virions were not added to any of the liquid media. Previous experiments indicated that adding virions to the media did not affect particle size or distribution (Bohannon and Lackemeyer, unpublished data). Variable spinning-top speeds, glycerol concentrations, and FBS concentrations were the experimental test parameters chosen for comparison with the four media.

For our experiments, the CenTAG™ was plumbed directly to the delivery line of a NHP head-only aerosol exposure chamber (Figure 3). An aerosol management platform (AeroMP, Biaera Technologies, USA) was used to conduct the tests within a Class III BSC. The resulting aerosol-particle sizes were measured with an aerodynamic particle sizer (APS, model 3321; TSI Inc., Shoreview, MN) spectrometer that provides high-resolution, real-time aerodynamic measurements of particles ranging from 0.5 to 20 μm in diameter. APS aerosol particles generated were collected, sized, and counted by the APS, and sizes were represented as mass median aerodynamic diameter (MMAD) with a geometric standard deviation (GSD). Using APS software, we analyzed particle mass, particle distribution, and particle concentration. The APS was attached by a sample line and oriented away from the head-only exposure chamber for visual purposes only. During aerosol acquisition, the APS was plumbed directly to the head-only chamber and near the breathing zone of the animal. A longer sample line could have created sharp turns or bends that would have caused the larger aerosol particles to impact the sample line and provide false readings.

Results

By exploring variables, such as the spinning top (disk) speed, glycerol concentration, and FBS concentration (solely or in combination) with four media, we generated a range of large-aerosol-particle sizes and distributions with CenTAG. APS recorded GSDs of ≤1.5 for all the particle size ranges tested. The CenTAG™ siphon vacuum eliminated the majority of the smaller satellite aerosol particles; however, some satellite aerosol particles escaped the siphon vacuum and entered the head-only exposure chamber. For each test parameter, we recorded in triplicate the three parameters (MMAD, GSD, particle count) using APS, and documented mean values for each data point. Particles sampled by the APS were taken over 5 minutes to ensure that the steady-state size of the aerosol was consistent and well characterized. A representative APS particle mass-weighted diameter distribution (Figure 2) was obtained using DMEM in 5% glycerol with a top (disk) rotor speed of 11 100 rpm. The resulting MMAD and GSD was 7.64 μm and 1.33, respectively.

The APS measurements revealed a relationship between created particle sizes using the four different test liquid media (DMEM, EMEM, RPMI, PBS), the addition of FBS, and the addition of glycerol (percent concentrations), and the spinning top (disk) speed. We verified that increasing the maximum rotor speed led to smaller aerosol particles sizes, increased aerosol particle counts, and increased GSD. The addition of glycerol to the four test media increased the surface tension and enabled formation of larger aerosol particles as indicated by MMAD for all tests performed. With increases in glycerol concentrations, a wider particle distribution was noted as indicated by increased GSD. However, at the same rotor speed, the GSD following the addition of glycerol was similar to that observed with liquid

media without glycerol. The results of MMAD, GSD, and aerosol particle counts for each liquid test medium, spinning top speed, and percentage of glycerol are presented in Tables 1–4.

The addition of FBS to the four test media decreased aerosol particle size compared to the standard media without FBS (data not shown). Consequently, FBS was not further pursued throughout the remainder of the experiments, and results of FBS addition to test media were omitted from this manuscript.

Discussion

We reported the CenTAG™ aerosol output characteristics for a range of targeted particle sizes and verified that all of the samples acquired and reported during our experimentation had an Event 2 value greater than 95%. During a gate window involving two signals, an Event 2 is a particle event in which the particle crosses above the detection threshold at the beginning of the first signal and at the end of the second signal. Any particles sampled by the APS that fall within an Event 2 bin are considered valid and not subject to coincidence or error (TSI., 2002). A target GSD of ≤1.2 was not successfully achieved during the CenTAG™ testing. Many culture media, such as DMEM, contain varieties of salts. We hypothesize that these media salts make it difficult to achieve a monodisperse aerosol during the generation of larger particles, due to the salts forming smaller satellite particles. To produce the desired GSD of ≤1.2, a virtual impactor could potentially be integrated into the exposure system to eliminate some on the smaller satellite particles (Marple and Chien, 1980). Virtual impactors separate particles by size into two airstreams. They are similar to conventional impactors, but the impaction surface is replaced with a virtual space of stagnant or slow moving air (Liebhaber et al., 1991). Large-aerosol particles continue downstream into the exposure chamber while small aerosol particles are diverted onto a collection surface. However, a GSD of ≤1.5 may be adequate for NHP aerosol research, provided that the large particles deposit in the upper respiratory regions of a NHP. Therefore, future NHP experiments will be performed to characterize the deposition pattern of CenTAG™-created aerosols. The use of several aerosol exposure modes (i.e., exposure to small and large-aerosol particles targeting lower and upper respiratory tract, respectively) could perhaps cover a wider spectrum of disease seen in humans and eventually allow the establishment of improved animal models for pathogenesis studies.

Conclusion

We have established a large-particle aerosol NHP exposure system based on CenTAG™ that is easily used within a Class III BSC where dexterity and space are limited. The CenTAG™ can be easily assembled and disassembled from within a Class III BSC for quick insertion and removal. By increasing the top (disk) rotor speed, smaller aerosol particles can be produced, while decreasing the rotor speed and increasing glycerol concentration in media facilitate formation of larger aerosol particles. The selection of particle size will depend on the target respiratory region for the infectious agent under investigation, and the CenTAG™ would be configured accordingly. Future large particle aerosol studies will be used to refine NHP infectious disease models and strive to establish infections that mimic human disease.

References

AEBERSOLD P. FDA experience with medical countermeasures under the Animal Rule. Adv Prev Med. 2012; 2012:507571. [PubMed: 21991452]

ALVES DA, GLYNN AR, STEELE KE, LACKEMEYER MG, GARZA NL, BUCK JG, MECH C, REED DS. Aerosol exposure to the Angola strain of Marburg virus causes lethal viral hemorrhagic fever in cynomolgus macaques. Vet Pathol. 2010; 47:831–51. [PubMed: 20807825]

BARNEWALL RE, FISHER DA, ROBERTSON AB, VALES PA, KNOSTMAN KA, BIGGER JE. Inhalational monkeypox virus infection in cynomolgus macaques. Front Cell Infect Microbiol. 2012; 2:117. [PubMed: 23061051]

BGI. Instruction Manual STAG 2000. Spinning Top Monodisperse Aerosol Generator Version 1.1. Waltham, MA: BGI; 2005. Available at: http://www.bgiusa.com/Manuals/stag_manual.pdf [Accessed on 8 October, 2014]

CENTERS FOR DISEASE CONTROL AND PREVENTION & NATIONAL INSTITUTES OF HEALTH. Biosafety in Microbiological and Biomedical Laboratories (BMBL). Washington, DC, USA: U.S. Government Printing Office; 2009. Available at: http://www.cdc.gov/biosafety/publications/bmbl5/ [Accessed on 8 October 2014]

CH TECHNOLOGIES USA. CenTag Centered Flow Tangential Aerosol Generator: Operation and Maintenance Manual, Version 1.0. Westwood, NJ: CH Technologies; 2013.

CHENG YS, IRSHAD H, KUEHL P, HOLMES TD, SHERWOOD R, HOBBS CH. Lung deposition of droplet aerosols in monkeys. Inhal Toxicol. 2008; 20:1029–36. [PubMed: 18720170]

DAVIES C, CHEAH P. Spinning generators of homogeneous aerosols. J Aerosol Sci. 1984; 15:719–739.

DAY WC, BERENDT RF. Experimental tularemia in *Macaca mulatta*: relationship of aerosol particle size to the infectivity of airborne *Pasteurella tularensis*. Infect Immun. 1972; 5:77–82. [PubMed: 4632469]

DRUETT HA, HENDERSON DW, PACKMAN L, PEACOCK S. Studies on respiratory infection. I. The influence of particle size on respiratory infection with anthrax spores. J Hyg (Lond). 1953; 51:359–71. [PubMed: 13096744]

EARLEY, EM.; JOHNSON, KM. The lineage of vero, vero 76, and its clone C1008 in the United States. In: SIMIZU, B.; TERASIMA, T., editors. Vero Cells: Origin, Properties, and Biomedical Applications. Tokyo, JP: Chiba University; 1988.

EGAN JR, HALL IM, LEACH S. Modeling inhalational tularemia: deliberate release and public health response. Biosecur Bioterror. 2011; 9:331–43. [PubMed: 22044315]

ELLISON JM. Adaptation of the spinning top generator to provide aerosols in the respirable range. Ann Occup Hyg. 1967; 10:363–7. [PubMed: 6063965]

FENNELLY KP, MARTYNY JW, FULTON KE, ORME IM, CAVE DM, HEIFETS LB. Cough-generated aerosols of *Mycobacterium tuberculosis*: a new method to study infectiousness. Am J Respir Crit Care Med. 2004; 169:604–9. [PubMed: 14656754]

FOOD AND DRUG ADMINISTRATION. Guidance for Industry and FDA Staff: Qualification Process for Drug Development Tools. Silver Spring, MD: Food and Drug Administration; 2014a. Available at http://www.fda.gov/downloads/Drugs/GuidanceComplianceRegulatoryInformation/Guidances/UCM230597.pdf [Accessed on 7 October 2014]

FOOD AND DRUG ADMINISTRATION. Draft Guidance. Silver Spring, MD: Food and Drug Administration; 2014b. Guidance for Industry: Product Development under the Animal Rule. Available at http://www.fda.gov/downloads/Drugs/GuidanceComplianceRegulatoryInformation/Guidances/UCM399217.pdf [Accessed on 7 October 2014]

GRALTON J, TOVEY E, MCLAWS ML, RAWLINSON WD. The role of particle size in aerosolised pathogen transmission: a review. J Infect. 2011; 62:1–13. [PubMed: 21094184]

GUSSMAN R. A further development of the May spinning top aerosol generator. Am Ind Hyg Assoc J. 1981; 42:208–212.

HARTMAN AL, POWELL DS, BETHEL LM, CAROLINE AL, SCHMID RJ, OURY T, REED DS. Aerosolized rift valley fever virus causes fatal encephalitis in african green monkeys and common marmosets. J Virol. 2014; 88:2235–45. [PubMed: 24335307]

HINDS, W. Aerosol Technology: Properties, Behavior, and Measurement of Airborne Particles. Hoboken, NJ: John Wiley & Sons; 1999.

HUANG J, MIKSZTA JA, FERRITER MS, JIANG G, HARVEY NG, DYAS B, ROY CJ, ULRICH RG, SULLIVAN VJ. Intranasal administration of dry powder anthrax vaccine provides protection against lethal aerosol spore challenge. Hum Vaccin. 2007; 3:90–3. [PubMed: 17375001]

LEE KM, CHIU KB, SANSING HA, DIDIER PJ, FICHT TA, ARENAS-GAMBOA AM, ROY CJ, MACLEAN AG. Aerosol-induced brucellosis increases TLR-2 expression and increased complexity in the microanatomy of astroglia in rhesus macaques. Front Cell Infect Microbiol. 2013; 3:86. [PubMed: 24350061]

LEFFEL EK, REED DS. Marburg and Ebola viruses as aerosol threats. Biosecur Bioterror. 2004; 2:186–91. [PubMed: 15588056]

LIEBHABER FB, LEHTIMÄKI M, WILLEKE K. Low-cost virtual impactor for large-particle amplification in optical particle counters. Aerosol Sci Technol. 1991; 15:208–213.

MARPLE VA, CHIEN CM. Virtual impactors: a theoretical study. Environ Sci Technol. 1980; 14:976–85. [PubMed: 22296546]

MAY KR. Spinning-top homogeneous aerosol generator with shockproof mounting. J Sci Instrum. 1966; 43:841–2. [PubMed: 5978866]

MAY KR. The collison nebulizer: Description, performance and application. J Aerosol Sci. 1973; 4:235–243.

MELTON P, HARRISON RM, BURNELL P. The evaluation of an improved spinning top aerosol generator and comparison with its predecessor. J Aerosol Sci. 1991; 22:101–110.

MITCHELL J, STONE R. Improvements to the May spinning-top aerosol generator. J Phys E: Sci Instrum. 1982; 15:565.

NALCA A, LIVINGSTON VA, GARZA NL, ZUMBRUN EE, FRICK OM, CHAPMAN JL, HARTINGS JM. Experimental infection of cynomolgus macaques (*Macaca fascicularis*) with aerosolized monkeypox virus. PLoS One. 2010; 5:e12880. [PubMed: 20862223]

RAABE OG, AL-BAYATI MA, TEAGUE SV, RASOLT A. Regional deposition of inhaled monodisperse coarse and fine aerosol particles in small laboratory animals. Ann Occup Hyg. 1988; 32:53–63.

REED DS, LACKEMEYER MG, GARZA NL, SULLIVAN LJ, NICHOLS DK. Aerosol exposure to Zaire ebolavirus in three nonhuman primate species: differences in disease course and clinical pathology. Microbes Infect. 2011; 13:930–6. [PubMed: 21651988]

REED DS, LARSEN T, SULLIVAN LJ, LIND CM, LACKEMEYER MG, PRATT WD, PARKER MD. Aerosol exposure to western equine encephalitis virus causes fever and encephalitis in cynomolgus macaques. J Infect Dis. 2005; 192:1173–82. [PubMed: 16136459]

ROY CJ, HALE M, HARTINGS JM, PITT L, DUNIHO S. Impact of inhalation exposure modality and particle size on the respiratory deposition of ricin in BALB/c mice. Inhal Toxicol. 2003; 15:619–38. [PubMed: 12692733]

THOMAS RJ. Particle size and pathogenicity in the respiratory tract. Virulence. 2013; 4:847–58. [PubMed: 24225380]

TSI. Model 3321 aerodynamic particle sizer spectometer: Instruction manual. Shoreview, MN: TSI; 2002. Available at: ftp://bbc.knmi.nl/BBC2/cabauw/other/tnofel/prog/doc/APS-3321.pdf [Accessed on 29 January, 2015]

WALTON W, PREWETT W. The production of sprays and mists of uniform drop size by means of spinning disc type sprayers. Proc Phys Soc, London, Sect B. 1949; 62:341.

YEAGER JJ, FACEMIRE P, DABISCH PA, ROBINSON CG, NYAKITI D, BECK K, BAKER R, PITT ML. Natural history of inhalation melioidosis in rhesus macaques (*Macaca mulatta*) and African green monkeys (*Chlorocebus aethiops*). Infect Immun. 2012; 80:3332–40. [PubMed: 22778104]

YOUNG HW, LARSON EW, DOMINIK JW. Modified spinning top homogeneous spray apparatus for use in experimental respiratory disease studies. Appl Microbiol. 1974; 28:929–34. [PubMed: 4451375]

ZUMBRUN EE, BLOOMFIELD HA, DYE JM, HUNTER TC, DABISCH PA, GARZA NL, BRAMEL NR, BAKER RJ, WILLIAMS RD, NICHOLS DK, NALCA A. A characterization of

aerosolized Sudan virus infection in African green monkeys, cynomolgus macaques, and rhesus macaques. Viruses. 2012; 4:2115–36. [PubMed: 23202456]

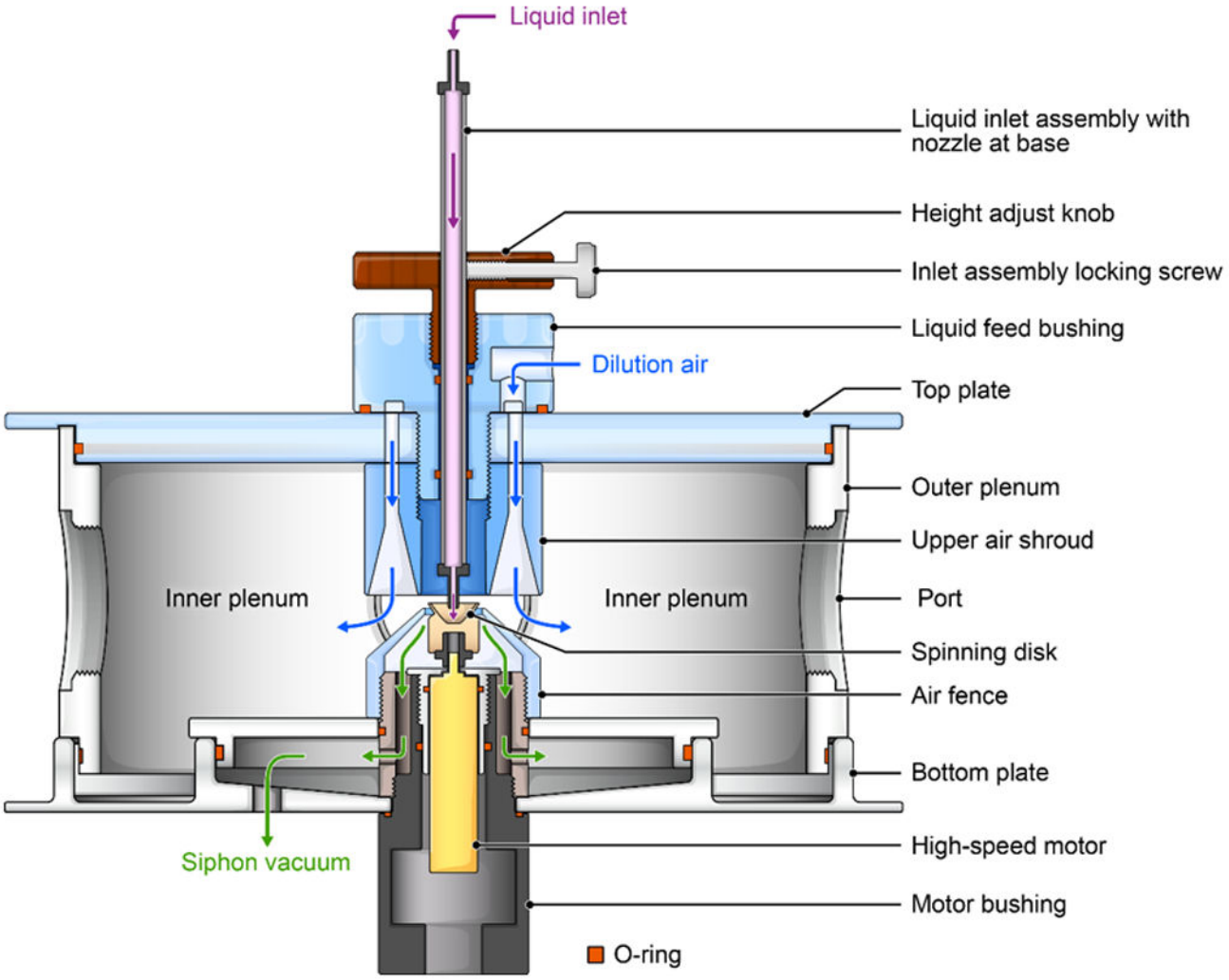

Figure 1.

Principles of operation of the center flow tangential aerosol generator. To create aerosol particles, liquid (pink arrow) is delivered onto the center of the rotating top through an inlet. A stream of dilution air (blue arrows), contained by a conical upper air shroud, is fed around the liquid feed nozzle to direct airflow around the upper edge of the spinning top (≤80,000 rpm). An adjustable height fence (with openings) surrounds the top and continues about 1–1.5 mm below the top. A siphon vacuum (green arrows) pulls the air stream through the fence at various fractions of the inlet flow rate. This airflow is optimized to entrain and remove the smaller satellite particles while permitting the larger particles to continue into the aerosol chamber. Two observation ports are within the plenum and fitted with polycarbonate inserts. rpm = revolutions per minute.

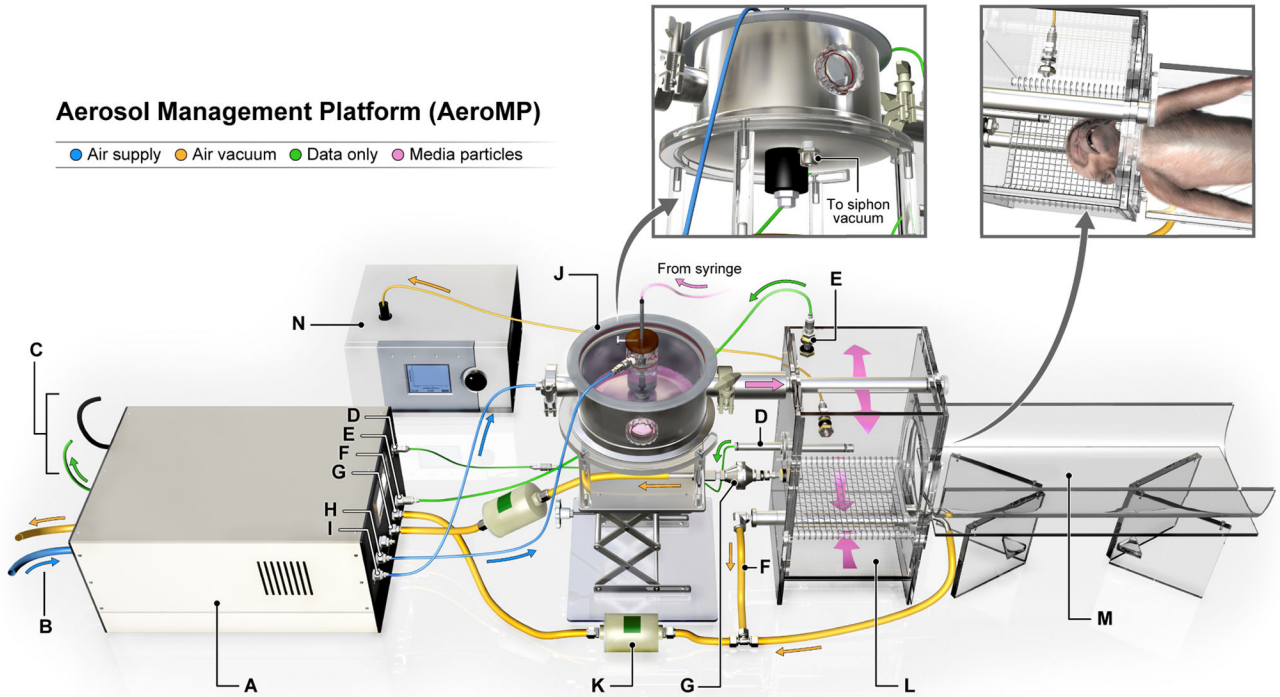

Figure 2.

Mass-weighted particle diameter distribution of generated particles calculated with APS software. Experimental parameters: DMEM in 5% glycerol with a top (disk) rotor speed of 11 100 rpm. DMEM = Dulbecco's Modified Eagle Medium; rpm = revolutions per minute.

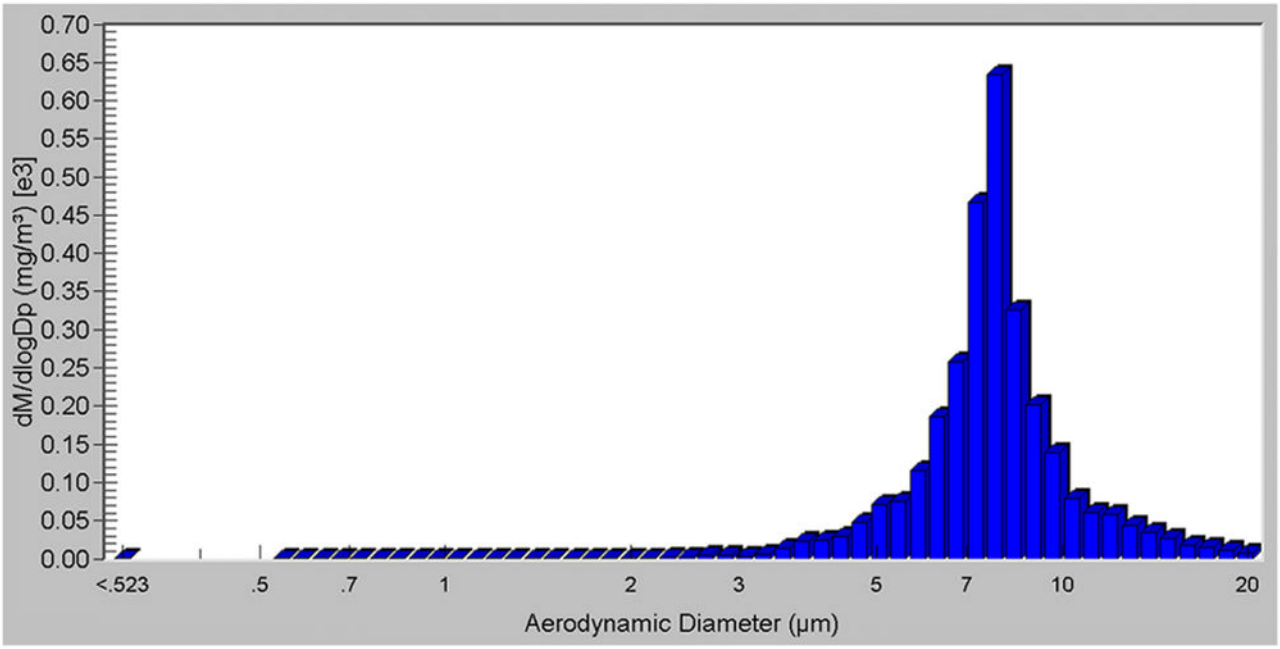

Figure 3.

The aerosol management platform. Labeled components are defined as follows: A. Biaera system - Controls, monitors, and records relative humidity and chamber pressure. Flow controllers and sensors monitor temperature, input airflow, and exhaust airflow in real time. B. AeroMP dedicated air supply and exhaust - Filters incoming BSC Class III air supply once, and expelled vacuum exhaust twice at laboratory HEPA deck mezzanine. C. Ethernet & power - Connects to sealed Ethernet port and electrical socket in BSC III. All AeroMP system functions are managed with dedicated AeroMP control software running on a personal computer in the laboratory. D. Temperature & humidity sensor - Monitors and displays the temperature and relative humidity within the exposure chamber. E. Pressure sensor - Monitors the pressure of the exposure chamber. The chamber pressure can be positive (outward) or negative (inward) depending on parameters determined by the researcher. F. Exhaust - Draws the particles through the exposure chamber using a HEPA filtered vacuum source, maintaining a balanced and dynamic flow rate. G. Sampler - Collects generated particles to determine the viral titer during the exposure. Utilizes a HEPA-filtered vacuum source to sample particles during the exposure. H. Dilution air - Additional air dilutes air from generator to ensure uniform distribution of air within the chamber. The overall flow rate is determined by the volume of the exposure chamber. I. Generator - Provides airflow to the CenTAG™. J. CenTAG™ - Generates large-aerosol particles containing virus from liquid media that is delivered during aerosol exposure. K. HEPA filter - Traps and contains expelled particulates from the exposure chamber’s exhaust ports. L. Head-only exposure chamber - Supports NHP head and contains generated particles within a 16-L chamber. M. NHP ramp - Supports NHP body in supine position throughout aerosol exposure. N. Aerodynamic particle sizer - Provides high-resolution, real-time aerodynamic measurements of particles from 0.5 to 20 µm, which allows the researcher to determine deposition within the respiratory tract. AeroMP = aerosol management platform;

BSC = biosafety cabinet; CenTAG = center flow tangential aerosol generator; HEPA = high efficiency particulate air; NHP = nonhuman primate.

Table 1

Effect of changes in DMEM media composition and rotor speed on particle size and counts.

Rotor Speed (rpm)[a]	Media (v v-1)	MMAD (μm)	GSD	Particle Counts (No. [cm^3]-1)
6960	DMEM	6.83	1.30	7.53E+04
11 100	DMEM	6.46	1.34	2.30E+05
15 200	DMEM	6.03	1.38	3.77E+05
23 450	DMEM	5.67	1.42	5.77E+05
31 780	DMEM	5.69	1.44	6.80E+05
6960	DMEM + 5% Glycerol	8.30	1.31	7.07E+04
11100	DMEM + 5% Glycerol	7.64	1.33	2.23E+05
15 200	DMEM + 5% Glycerol	7.19	1.36	3.93E+05
23 450	DMEM + 5% Glycerol	7.00	1.40	6.20E+05
31 780	DMEM + 5% Glycerol	6.98	1.41	5.33E+05
6960	DMEM + 10% Glycerol	9.60	1.35	6.83E+04
11 100	DMEM + 10% Glycerol	8.33	1.33	2.20E+05
15 200	DMEM + 10% Glycerol	7.97	1.36	3.93E+05
23 450	DMEM + 10% Glycerol	7.77	1.39	6.20E+05
31 780	DMEM + 10% Glycerol	7.72	1.40	7.40E+05
6960	DMEM + 20% Glycerol	10.97	1.39	7.13E+04
11 100	DMEM + 20% Glycerol	9.10	1.34	1.87E+05
15 200	DMEM + 20% Glycerol	8.82	1.35	3.43E+05
23 450	DMEM + 20% Glycerol	8.37	1.36	4.70E+05
31 780	DMEM + 20% Glycerol	8.21	1.37	4.87E+05

[a]Rotating speed of the top shaft is expressed in rpm rather than *g*, as the liquid is accelerating at different speeds across the surface of the top.

Table 2

Effect of changes in EMEM media composition and rotor speed on particle size and counts.

Rotor Speed (rpm)[a]	Media (v v-1)	MMAD (μm)	GSD	Particle Counts (No. [cm^3]-1)
6960	EMEM	6.38	1.33	1.03E+05
11 100	EMEM	5.49	1.39	3.40E+05
15 200	EMEM	5.14	1.44	5.07E+05
23 450	EMEM	4.83	1.49	7.27E+05
31 780	EMEM	4.77	1.51	8.13E+05
6960	EMEM + 5% Glycerol	8.35	1.34	6.97E+04
11 100	EMEM + 5% Glycerol	7.66	1.34	2.03E+05
15 200	EMEM + 5% Glycerol	7.42	1.37	3.40E+05
23 450	EMEM + 5% Glycerol	7.23	1.39	5.17E+05
31 780	EMEM + 5% Glycerol	7.18	1.40	6.27E+05
6960	EMEM + 10% Glycerol	9.78	1.35	5.17E+04
11 100	EMEM + 10% Glycerol	8.64	1.38	1.93E+05
15 200	EMEM + 10% Glycerol	8.25	1.38	3.67E+05
23 450	EMEM + 10% Glycerol	8.03	1.40	5.40E+05
31 780	EMEM + 10% Glycerol	7.90	1.41	6.70E+05
6960	EMEM + 20% Glycerol	11.53	1.38	6.70E+04
11 100	EMEM + 20% Glycerol	9.70	1.38	2.03E+05
15 200	EMEM + 20% Glycerol	9.07	1.40	3.80E+05
23 450	EMEM + 20% Glycerol	8.61	1.42	5.97E+05
31 780	EMEM + 20% Glycerol	8.55	1.43	6.63E+05

[a]Rotating speed of the top shaft is expressed in rpm rather than *g*, as the liquid is accelerating at different speeds across the surface of the top.

Table 3

Effect of changes in RPMI media composition and rotor speed on particle size and counts.

Rotor Speed (rpm)[a]	Media (v v-1)	MMAD (um)	GSD	Particle Counts (No. [cm^3]-1)
6960	RPMI	6.35	1.31	6.97E+04
11 100	RPMI	5.91	1.36	2.67E+05
15 200	RPMI	5.60	1.40	3.67E+05
23 450	RPMI	5.32	1.44	4.97E+05
31 780	RPMI	5.24	1.45	5.87E+05
6960	RPMI + 5% Glycerol	8.31	1.35	6.00E+04
11 100	RPMI + 5% Glycerol	7.25	1.37	2.27E+05
15 200	RPMI + 5% Glycerol	7.13	1.38	3.73E+05
23 450	RPMI + 5% Glycerol	7.00	1.41	5.57E+05
31 780	RPMI + 5% Glycerol	6.84	1.43	6.80E+05
6960	RPMI + 10% Glycerol	9.73	1.37	6.17E+04
11 100	RPMI + 10% Glycerol	8.27	1.37	2.10E+05
15 200	RPMI + 10% Glycerol	7.91	1.40	3.70E+05
23 450	RPMI + 10% Glycerol	7.70	1.41	5.57E+05
31 780	RPMI + 10% Glycerol	7.63	1.43	6.77E+05
6960	RPMI + 20% Glycerol	11.30	1.37	7.40E+04
11 100	RPMI + 20% Glycerol	10.30	1.36	1.93E+05
15 200	RPMI + 20% Glycerol	9.61	1.38	3.53E+05
23 450	RPMI + 20% Glycerol	9.26	1.40	4.37E+05
31 780	RPMI + 20% Glycerol	9.02	1.41	5.70E+05

[a]Rotating speed of the top shaft is expressed in rpm rather than *g*, as the liquid is accelerating at different speeds across the surface of the top.

Table 4

Effect of changes in PBS media composition and rotor speed on particle size and counts.

Rotor Speed (rpm)[a]	Media (v v-1)	MMAD (um)	GSD	Particle Counts (No. [cm^3]-1)
6960	PBS	6.77	1.32	9.77E+04
11 100	PBS	5.79	1.37	2.70E+05
15 200	PBS	5.38	1.40	4.23E+05
23 450	PBS	5.17	1.45	6.03E+05
31 780	PBS	5.03	1.46	6.90E+05
6960	PBS + 5% Glycerol	8.47	1.35	7.43E+04
11 100	PBS + 5% Glycerol	7.56	1.35	2.27E+05
15 200	PBS + 5% Glycerol	7.42	1.36	3.63E+05
23 450	PBS + 5% Glycerol	7.26	1.38	5.80E+05
31 780	PBS + 5% Glycerol	7.25	1.39	6.73E+05
6960	PBS + 10% Glycerol	9.12	1.34	7.30E+04
11 100	PBS + 10% Glycerol	8.31	1.33	2.10E+05
15 200	PBS + 10% Glycerol	8.10	1.35	3.62E+05
23 450	PBS + 10% Glycerol	7.87	1.38	5.37E+05
31 780	PBS + 10% Glycerol	7.71	1.39	6.70E+05
6960	PBS + 20% Glycerol	11.80	1.38	5.97E+04
11 100	PBS + 20% Glycerol	9.28	1.37	1.83E+05
15 200	PBS + 20% Glycerol	8.82	1.37	3.47E+05
23 450	PBS + 20% Glycerol	8.62	1.38	5.27E+05
31 780	PBS + 20% Glycerol	8.52	1.40	6.63E+05

[a] Rotating speed of the top shaft is expressed in rpm rather than *g*, as the liquid is accelerating at different speeds across the surface of the top.